ACS Chemical Neuroscience
Cite This: ACS Chem. Neurosci. 2019, 10, 460−471
Research Article
pubs.acs.org/chemneuro

Single Quantum Dot Imaging Reveals PKCβ-Dependent Alterations in Membrane Diffusion and Clustering of an Attention-Deficit Hyperactivity Disorder/Autism/Bipolar Disorder-Associated Dopamine Transporter Variant

Lucas B. Thal,[†,⊥] Ian D. Tomlinson,[†] Meagan A. Quinlan,[▽,○] Oleg Kovtun,[†] Randy D. Blakely,[▽,○] and Sandra J. Rosenthal*[,†,‡,§,∥,⊥,#]

[†]Department of Chemistry, [‡]Department of Pharmacology, [§]Department of Chemical and Biomolecular Engineering, [∥]Department of Physics and Astronomy, [⊥]Vanderbilt Institute of Chemical Biology, and [#]Vanderbilt Institute of Nanoscale Science and Engineering, Vanderbilt University, Nashville, Tennessee 37235, United States

[▽]Department of Biomedical Science and [○]FAU Brain Institute, Florida Atlantic University, Jupiter, Florida 33458, United States

Supporting Information

ABSTRACT: The dopamine transporter (DAT) is a transmembrane protein that terminates dopamine signaling in the brain by driving rapid dopamine reuptake into presynaptic nerve terminals. Several lines of evidence indicate that DAT dysfunction is linked to neuropsychiatric disorders such as attention-deficit/hyperactivity disorder (ADHD), bipolar disorder (BPD), and autism spectrum disorder (ASD). Indeed, individuals with these disorders have been found to express the rare, functional DAT coding variant Val559, which confers anomalous dopamine efflux (ADE) *in vitro* and *in vivo*. To elucidate the impact of the DAT Val559 variant on membrane diffusion dynamics, we implemented our antagonist-conjugated quantum dot (QD) labeling approach to monitor the lateral mobility of single particle-labeled transporters in transfected HEK-293 and SK-N-MC cells. Our results demonstrate significantly higher diffusion coefficients of DAT Val559 compared to those of DAT Ala559, effects likely determined by elevated N-terminal transporter phosphorylation. We also provide pharmacological evidence that PKCβ-mediated signaling supports enhanced DAT Val559 membrane diffusion rates. Additionally, our results are complimented with diffusion rates of phosphomimicked and phosphorylation-occluded DAT variants. Furthermore, we show DAT Val559 has a lower propensity for membrane clustering, which may be caused by a mutation-derived shift out of membrane microdomains leading to faster lateral membrane diffusion rates. These findings further demonstrate a functional impact of DAT Val559 and suggest that changes in transporter localization and lateral mobility may sustain ADE and contribute to alterations in dopamine signaling underlying multiple neuropsychiatric disorders.

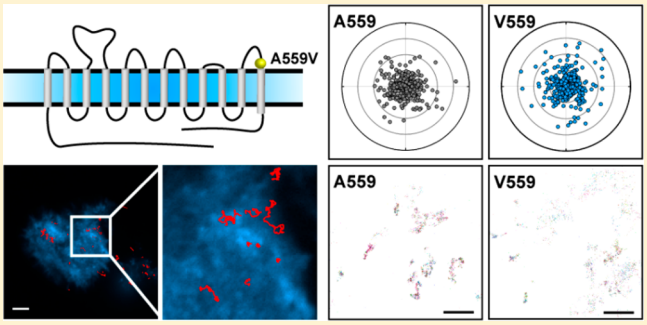

KEYWORDS: *Attention-deficit/hyperactivity disorder, bipolar disorder, clustering, single quantum dot tracking, dopamine transporter, single molecule imaging*

INTRODUCTION

The catecholamine neurotransmitter dopamine is central to the modulation of neuronal pathways that control diverse behaviors including those linked to movement, reward, mood, attention, and cognition.[1,2] Disrupted dopamine signaling is associated with multiple brain disorders such as Parkinson's disease (PD), schizophrenia, bipolar disorder (BPD), attention-deficit/hyperactive disorder (ADHD), and addiction.[3−6] The presynaptic Na^+/Cl^- coupled dopamine transporter (DAT) determines dopamine signaling amplitude and duration by actively clearing synaptic dopamine following vesicular release.[7−9] Importantly, genetic polymorphisms of the human DAT gene (*DAT1*, *SLC6A3*) have been identified in cases of ADHD, BPD, autism spectrum disorder (ASD), PD, and juvenile dystonia.[10−15] DAT endocytic trafficking at presynaptic terminals is likely a major regulatory mode of synaptic strength in dopamine neurons,[16−19] a process that can be referred to as vesicle trafficking, wherein DAT proteins are moved into and out of the plasma membrane from intracellular compartments. Consequently, constitutive and regulated vesicle trafficking is considered to be the principal determinant of functional DAT availability, though engagement of these mechanisms appears to be region dependent.[20,21] DAT proteins can also engage cell surface trafficking or lateral

Received: July 13, 2018
Accepted: August 28, 2018
Published: August 28, 2018

DOI: 10.1021/acschemneuro.8b00350
ACS Chem. Neurosci. 2019, 10, 460−471

membrane diffusion that can be impacted by DAT-associated proteins and disease-associated mutations revealed by total internal reflection fluorescence (TIRF) microscopy,[22,23] fluorescence recovery after photobleaching (FRAP),[24] and single particle tracking (SPT) techniques.[25,26]

Single molecule imaging offers information such as kinetics and dynamics of molecules in real-time, which would be lost in conventional ensemble measurements. The study of lateral diffusion at a single protein level requires an approach that uses bright probes, such as quantum dots (QD), to achieve signal-to-noise ratios suitable for high spatiotemporal resolution. QDs exhibit unique photophysical properties that make them an attractive first choice for single molecule imaging applications,[27] which many groups have employed to investigate the diffusion dynamics of single transmembrane, neurotransmitter receptors, and transporter proteins (e.g., GABA receptors, glycine receptors, serotonin transporters, DAT).[26,28−32] First, QDs offer a prolonged photostability required for imaging acquisition times on the order of minutes.[27] Second, QDs have broad absorption spectra and size-tunable narrow Gaussian photoluminescence profiles that permit simultaneous multicolor tracking with little to no spectral bleedthrough. As a product of high quantum yields and large absorption cross sections, QDs are also very bright upon laser irradiation.[33] Together, these properties have enabled the detection of single proteins in living cells targeted by antagonist- and antibody-conjugated biocompatible QDs.[27,34] Because surface trafficking is believed to be a critical posttranslational regulatory mechanism,[35−37] our group developed an antagonist-conjugated QD labeling approach to monitor individual membrane proteins in live cells (Figure 1).[38−41] Subsequently,

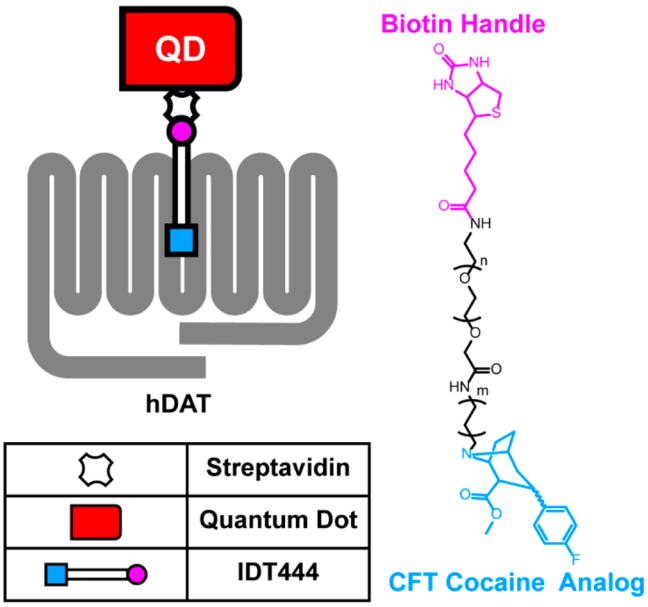

Figure 1. Schematic outlining single QD-DAT labeling architecture and chemical structure of the DAT-specific IDT444 affinity tool.

we reported that the ADHD-associated DAT Cys615 coding variant exhibited significantly increased membrane mobility and a pronounced lack of dynamic response to lipid raft disruption and amphetamine (AMPH) stimulation.[26]

Along with Cys615 as one of the multiple genetic DAT variants, a second variant, Val559, has been identified in subjects with distinct disorders associated with dopamine signaling dysfunction. The Val559 mutation was first identified in a female proband presenting with BPD[11] followed by its detection in two brothers with ADHD[10] and subsequently in two unrelated adolescent males with ASD.[42] Studies with mice expressing the DAT Val559 variant demonstrate elevated extracellular dopamine levels, altered biochemical and behavioral responses to psychostimulants, and changes in behaviors linked to reward and impulsivity circuits.[43,44] In reduced preparations, the mutant transporter displays multiple, striking phenotypes. Mazei-Robison and colleagues demonstrated that the Val559 mutation, though not impacting DAT surface expression or dopamine uptake, induces anomalous dopamine efflux (ADE), whereby mutant transporters spontaneously move dopamine from the cytosol to the extracellular space.[45] DAT Val559 also demonstrates elevated levels of N-terminal phosphorylation at distal Ser residues.[42] Mutation of these sites eliminates ADE, suggesting that N-terminal phosphorylation plays an essential role in sustaining dopamine reverse transport. Whether ADE is induced directly by transporter phosphorylation or is a consequence of changes in membrane distribution, lateral membrane trafficking, and/or the spatiotemporal organization of DAT with membrane partners is unclear. Here, we implemented our dynamic QD-based DAT monitoring approach to examine the impact of the DAT Val559 mutation on DAT membrane diffusion dynamics. We demonstrate that DAT exhibits increased lateral mobility in transiently transfected HEK-293 and SK-N-MC cells, movements that are also sensitive to mutations and pharmacological approaches impacting DAT phosphorylation. Using tracking and localization microscopy (TALM) and an intensity-based clustering analysis we developed, we demonstrate that the mutant targets to surface membrane clusters of HEK-293 cells to a lesser degree than the wild-type transporter. Our findings support the idea that disruption of normal DAT spatiotemporal organization may impose elevated risk for neuropsychiatric disorders linked to perturbed dopamine signaling.

RESULTS AND DISCUSSION

Single QD Tracking Analysis Reveals DAT Val559 Has Aberrant Membrane Diffusion Dynamics. DAT Val559 has been reported to display altered vesicle trafficking *in vitro* and *in vivo*.[21,42] To assess the impact of the DAT Val559 mutation on lateral membrane trafficking, we targeted DATs with DAT antagonist-conjugated QDs.[40] Figure 1 illustrates the chemical structure of IDT444, the DAT-specific ligand used in our labeling paradigm, which makes use of the high-affinity carbomethoxy-fluorophenyl cocaine analog β-CFT (also known as WIN 35,428), an 11-carbon alkyl spacer to allow the antagonist to access its DAT binding site, and a PEG linker connected to a biotin molecule to provide for streptavidin-mediated QD binding.[40] This QD-IDT444 labeling strategy has proven successful in single QD tracking of DAT proteins.[26,40] At concentrations of 100 nM IDT444 and <0.1 nM QD, we previously demonstrated that nonspecific binding was virtually eliminated.[26,40] Because DAT Val559 is similar to wild-type DAT Ala559 in both β-CFT binding affinity and cocaine inhibition of [^{3}H]-DA uptake,[46,47] we expect IDT444 labeling to be comparable across cells expressing DAT Ala559 or Val559. Because dopamine D2 receptors (D2Rs) physically associate with DAT and promote DAT Val559-induced ADE,[48−50] we pursued studies of multiple DAT variants (e.g., A559V, YFPDAT, YFPDAT S/

DOI: 10.1021/acschemneuro.8b00350
ACS Chem. Neurosci. 2019, 10, 460−471

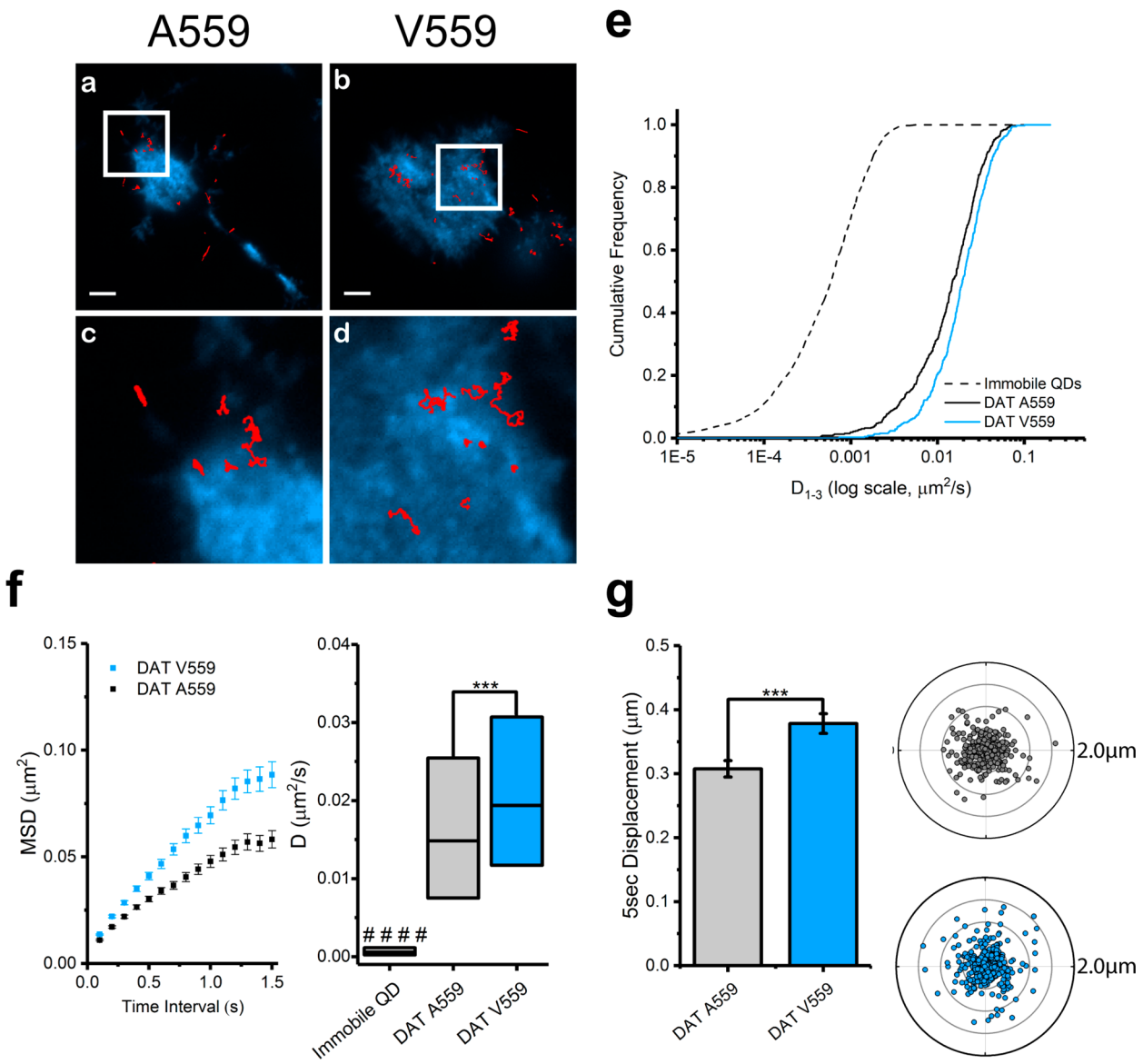

Figure 2. DAT Val559 exhibits faster mobility compared to that of DAT Ala559 transiently expressed in HEK-293 cells. (a,b) Representative trajectories collected over 60 s of QD-bound DAT and DAT Val559 coding variants superimposed to the IDT307 channel (scale bar = 5 μm). (c,d) Images at 4× magnification of images in a and b, respectively. (e) Cumulative frequency distributions of diffusion coefficients (D_{1-3}) of immobile QDs, DAT Ala559, and DAT Val559 (Kolmogorov−Smirnov 2-sample test, $p < 0.0001$). (f) Averaged mean square displacement (MSD) plots (mean ± S.E.M.) and diffusion coefficient box plots (median, 25% and 75% interquartiles, one-way ANOVA followed by Bonferroni's multiple comparison test, $^{***}p < 0.001$, $^{\#\#\#\#}p < 0.001$ comparing data sets to immobilized QDs as control) of trajectories analyzed for DAT Ala559 and DAT Val559. (g) A 5 s displacement bar graph (mean ± S.E.M., unpaired Student's t test, $^{***}p < 0.001$) and polar plots (outer radius limit = 2 μm) of single DAT Ala559 (gray) and DAT Val559 (blue). DAT displacements are normalized to their spatial origin. N (trajectories) are provided in Table S1.

D, DAT S53A, DAT S53D, A559V + S53A, A559V + S53D) in HEK-293 cells that endogenously express D2Rs.[50] QD-labeled human DAT Ala559 and human DAT Val559 were studied in live, transiently transfected HEK-293 cells and imaged using TIRF microscopy at 10 hz (see Movie S1 for a representative time series). Representative trajectories for both DAT Ala559 and DAT Val559 coding variants are shown in Figure 2a and b. IDT307 (4-(4-dimethylamino)phenyl-1-methylpyridinium, APP+),[51,52] a DAT-specific fluorescent analog of 1-methyl-4-phenylpyridinium (MPP+), was used to outline the cell boundaries (Figure 2a−d). Diffusion coefficients (D_{1-3}, see Materials and Methods for details on calculations and analysis) were determined for populations of DAT Ala559 and DAT Val559 trajectories. Cumulative probability distributions (Figure 2e) of D_{1-3} values reveal a significant increase in DAT Val559 diffusion rates under basal conditions as compared to DAT Ala559. Averaged mean square displacement (MSD) curves show confined motion for both DAT Ala559 and DAT Val559, though the Val559 slope is significantly larger than the wild-type. DAT Val559 D_{1-3} interquartile ranges (25−75%) are also significantly greater than DAT Ala559 (Figure 2f). In addition to diffusion coefficients, 5 s radial displacement vectors were calculated by obtaining QD particle distance and direction traveled in 5 s (50 frames at 10 Hz) normalized to the particle position at the first frame (see Materials and Methods). Averaged 5 s

DOI: 10.1021/acschemneuro.8b00350
ACS Chem. Neurosci. 2019, 10, 460−471

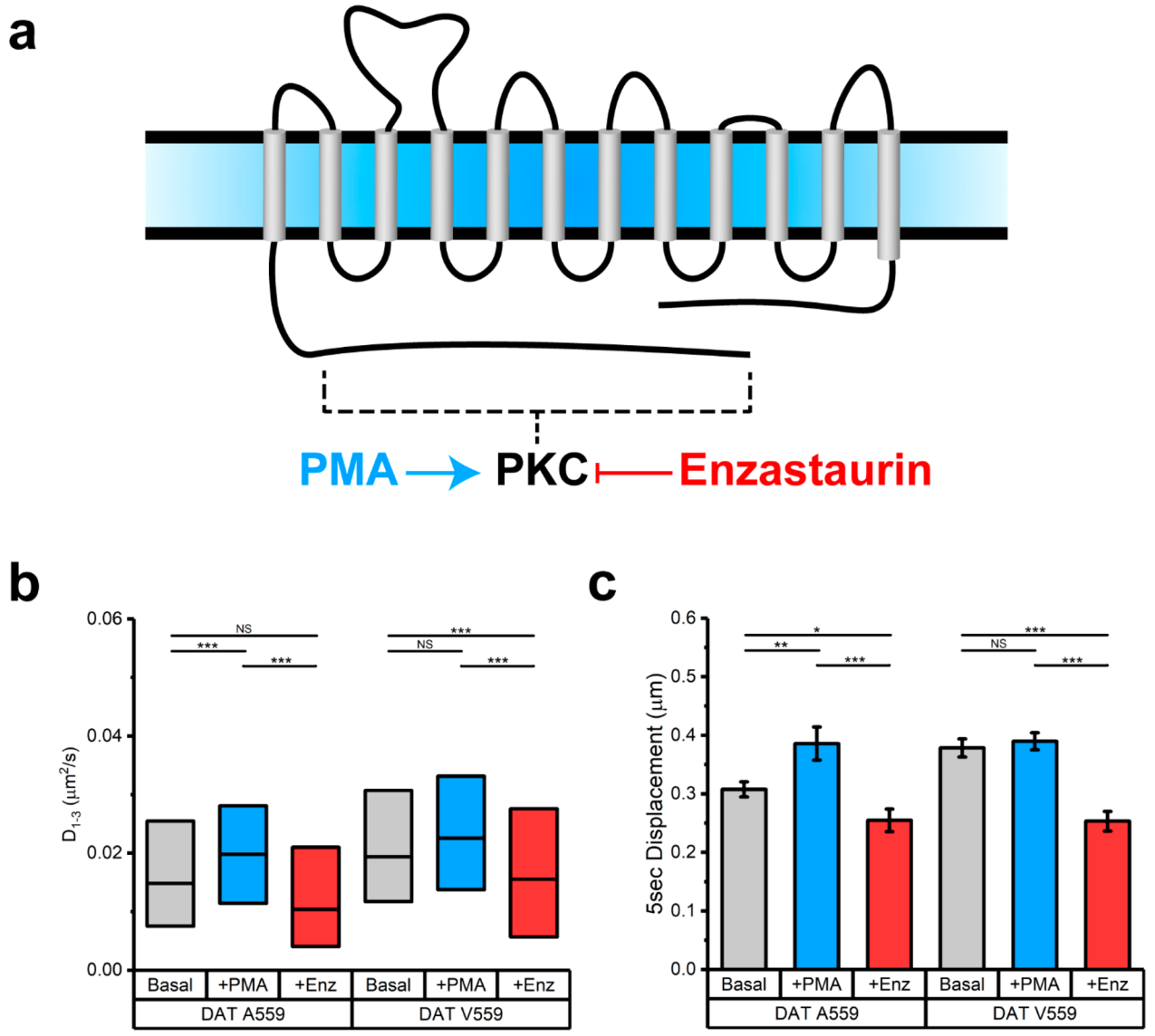

Figure 3. DAT Val559 diffusion is unresponsive to protein kinase C (PKC) activation and is attenuated by PKCβ inhibition in HEK-293 cells. (a) Schematic of DAT with PKC activation by PMA highlighted in blue and PKCβ inhibition by enzastaurin (Enz) highlighted in red. The dashed line denotes the general region of phosphorylation mediated by PKC activation. (b) Diffusion coefficient box plot (median, 25% and 75% interquantiles, one-way ANOVA followed by Bonferroni's multiple comparison test, NS $p > 0.05$, ***$p < 0.001$) of trajectories analyzed for DAT Ala559 and DAT Val559 under basal, stimulated (+PMA) conditions, and inhibited (+Enz) conditions. (c) A 5 s displacement bar graph (mean ± S.E.M., unpaired Student's t test, NS $p > 0.05$ *$p < 0.05$, **$p < 0.01$, ***$p < 0.001$) of trajectories analyzed for DAT Ala559 and DAT Val559 under basal, stimulated (+PMA), and inhibited (+Enz) conditions. N (trajectories) are provided in Table S1.

displacements for DAT Ala559 and DAT Val559 under basal conditions proved to be significantly different (Figure 2g). To increase the physiological relevance of our studies, we repeated our experiments using catecholaminergic neuroblastoma cells (SK-N-MC) derived from the human brain. Results in Figure S1 demonstrate findings similar to those in our HEK-293 studies using SK-N-MC cells expressing DAT Ala559 and DAT Val559.

DAT Val559 Membrane Mobility Is Insensitive to PMA-Triggered PKC Activation but Can Be Diminished by PKCβ Inhibition. DAT-mediated dopamine efflux and DAT surface density are impacted by protein kinase C (PKC) signaling.[5] To examine whether faster DAT Val559 mobility is associated with transporter phosphorylation status, we examined the effects of general PKC activation on DAT Ala559 and DAT Val559 mobility using phorbol-12-myristate-13-acetate (PMA), a diester that binds to the catalytic C1 domain of PKC, which leads to stimulation of PKC activity. HEK-293 cells were preincubated with 100 nM PMA for 30 min prior to QD labeling. PKC activation induced an increase in DAT Ala559 D_{1-3} and 5 s displacements. However, these effects of PMA were not observed for DAT Val559 (Figure 3b, c). Similar results to those observed in HEK-293 cells were obtained with transfected SK-N-MC cells, demonstrating consistency across cell lines (Figure S2).

PMA activates multiple PKC isoforms that can regulate DAT.[5] Because PKCβ regulates dopamine efflux,[53] PKCβ activity is elevated in DAT Val559 expressing HEK-293 cells,[42] and antagonism of PKCβ restores AMPH-induced DAT internalization,[54] we focused further studies on this PKC isoform. Specifically, we tested the ability of the PKCβ-specific inhibitor enzastaurin, previously shown to attenuate dopamine

DOI: 10.1021/acschemneuro.8b00350
ACS Chem. Neurosci. 2019, 10, 460−471

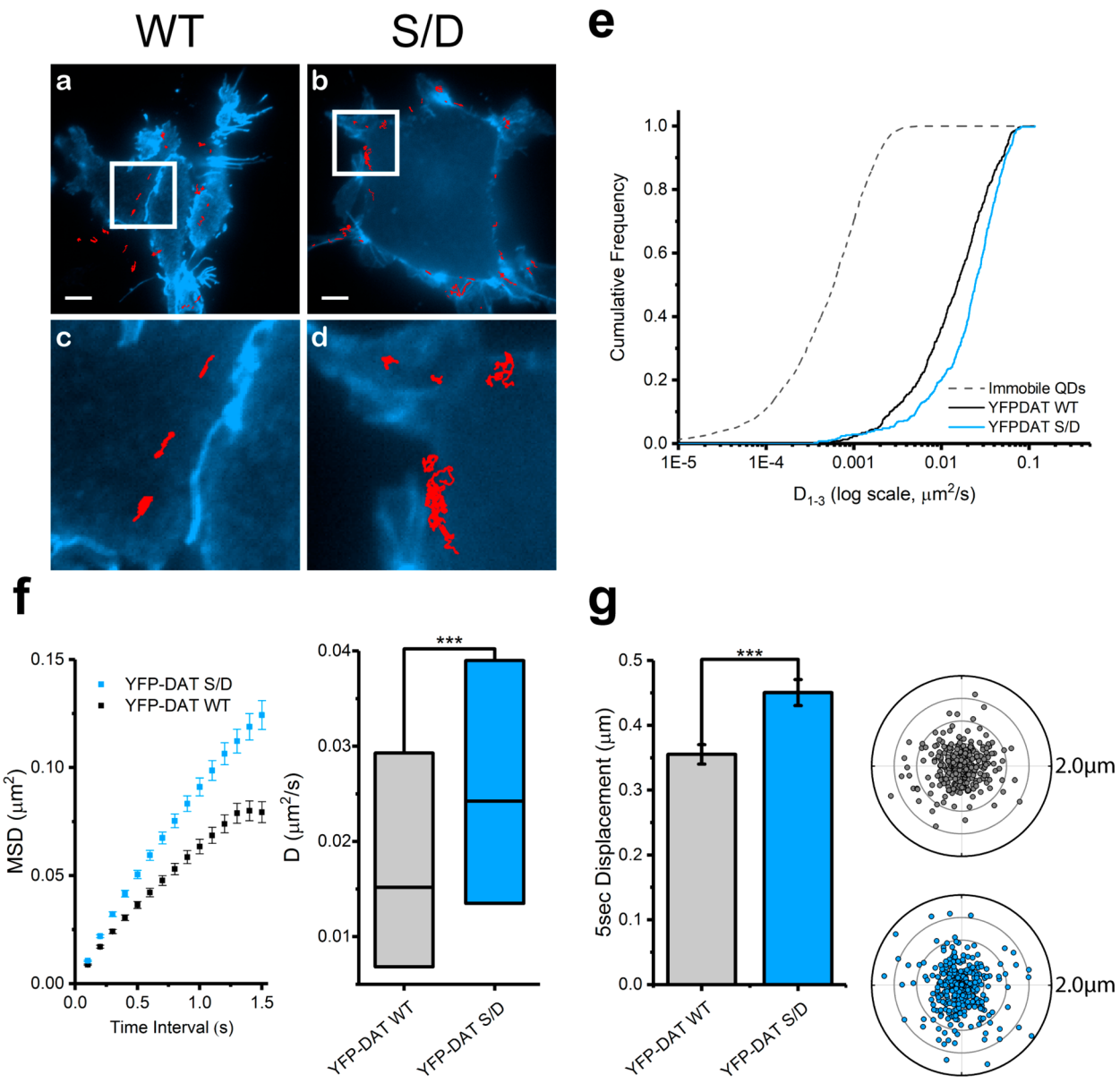

Figure 4. Phosphomimetic YFP-DAT S/D exhibits faster membrane mobility than that of wild-type YFP-DAT in HEK-293 cells. (a,b) Representative trajectories collected over 60 s of QD-bound YFP-DAT WT and YFP-DAT S/D superimposed to cell membranes outlined by YFP (scale bar = 5 μm). (c,d) Images at 4× magnification of images in a and b, respectively. (e) Cumulative frequency distributions of diffusion coefficients (D_{1-3}) of immobile QDs, YFP-DAT WT, and YFP-DAT S/D (Kolmogorov−Smirnov 2-sample test, $p< 0.0001$). (f) Averaged mean square displacement (MSD) plots (mean ± S.E.M.) and a diffusion coefficient box plot (median, 25% and 75% interquantiles, one-way ANOVA followed by Bonferroni's multiple comparison test, ***$p < 0.001$) of trajectories analyzed for YFP-DAT WT and YFP-DAT S/D. (g) A 5 s displacement bar graph (mean ± S.E.M., unpaired Student's t test, ***$p < 0.001$) and polar plots (outer radius limit = 2 μm) of single YFP-DAT WT (gray) and YFP-DAT S/D (blue). DAT-QD displacements are normalized to their spatial origin. N (trajectories) are provided in Table S1.

efflux *in vivo*,[55] to determine whether PKCβ activity supports enhanced DAT Val559 membrane diffusion. DAT Ala559 and DAT Val559 transfected cells were preincubated with 1 μM enzastaurin for 30 min prior to PMA treatment and QD labeling. Both DAT and DAT Val559 responded to PKCβ inhibition by reduced D_{1-3} and reduced 5 s displacements (Figure 3b, c). Similar results were obtained using SK-N-MC cells as well (Figure S2). These findings indicate that PKCβ tone exists in our cell models that supports basal DAT Ala559 and DAT Val559 lateral mobility and that PMA can further enhance wild-type but not mutant DAT lateral mobility in a PKCβ-dependent manner. Our findings are also consistent with a model whereby the elevated PKCβ activity reported in DAT Val559 transfected cells leads to elevated DAT phosphorylation and increased lateral mobility,[42] effects mimicked by treating DAT Ala559 expressing cells with PMA.

DAT Val559 has been shown to exhibit elevated phosphorylation of multiple N-terminal Ser residues, which is essential for DAT Val559 ADE.[50] We hypothesized that elevated Ser phosphorylation of the DAT Val559 N-terminus might also be involved in the enhanced lateral mobility of this variant. To test this idea, we evaluated the impact of phosphomimetic mutations of the N-termimal Ser residues on lateral mobility using our antagonist-coupled QD approach. Here, Ser residues were mutated to Asp residues (S/D), which are negatively charged at pH 7, thus mimicking a

DOI: 10.1021/acschemneuro.8b00350
ACS Chem. Neurosci. 2019, 10, 460−471

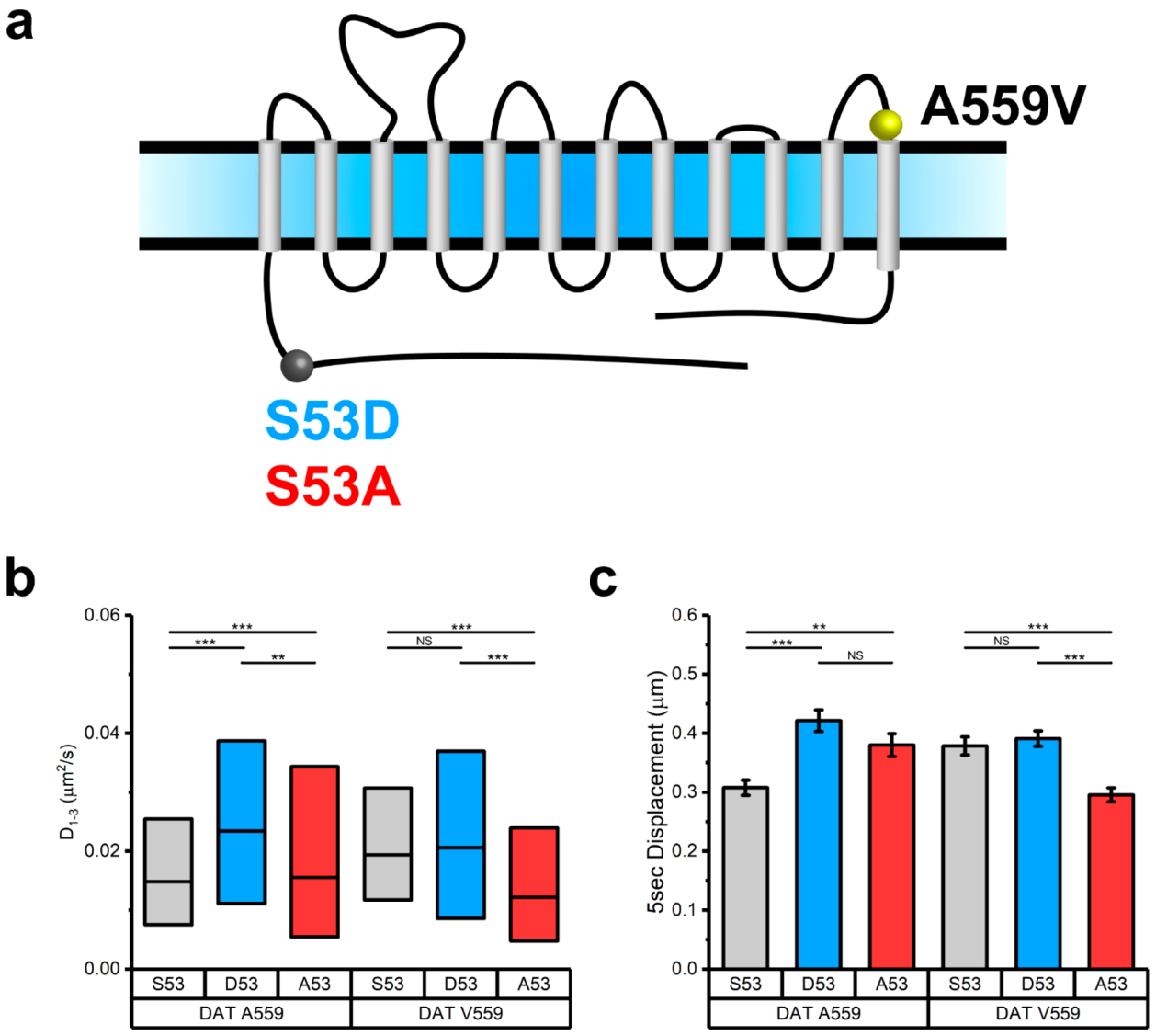

Figure 5. S53 phosphorylation alters mobility of DAT and DAT Val559. (a) Schematic of DAT and positions of variants tested. The A559V site is highlighted in yellow; S53A is highlighted in blue, and S53A is highlighted in red. (b) Diffusion coefficient box plot (median, 25% and 75% interquantiles, one-way ANOVA followed by Bonferroni's multiple comparison test, NS $p > 0.05$, $^{**}p < 0.01$ $^{***}p < 0.001$) of trajectories analyzed for Ser53, Asp53, and Ala53 under DAT Ala559 and DAT Val559 backgrounds. (c) A 5 s displacement bar graph (mean ± S.E.M., unpaired Student's *t* test, NS $p > 0.05$, $^{**}p < 0.01$, $^{***}p < 0.001$) of trajectories analyzed for Ser53, Asp53, and Ala53 under DAT Ala559 and DAT Val559 backgrounds. N (trajectories) are provided in Table S1.

phosphorylated state. We chose to use YFP-DAT and YFP-DAT S/D available for purchase from Addgene (see Materials and Methods) considering GFP and YFP moieties have been reported to induce no adverse effects on DAT function.[56,57] Representative trajectories of QD-labeled YFP-DAT S/D demonstrate a greater area explored compared to QD-labeled YFP-DAT (Figure 4a–d). In Figure 4e, the cumulative probability distribution plot of D_{1-3} clearly demonstrates an increase in YFP-DAT S/D diffusion rate compared to that of YFP-DAT. Complementing the mobility of DAT Val559, YFP-DAT S/D has elevated D_{1-3} and 5 s displacements compared to those of YFP-DAT. Results using SK-N-MC are in agreement with these data (Figure S3).

A559V-Induced Ser53 Phosphorylation Increases Membrane DAT Mobility. In addition to the phosphorylation of N-terminal Ser residues, juxtamembrane DAT residue Thr53 (Ser53 in humans) accounts for a portion of basal DAT phosphorylation in transfected cells and *in vivo*.[58] Phosphorylation of Thr53 has been reported to impact dopamine uptake and AMPH-induced efflux,[58] whereas spatiotemporal effects of Thr53 phosphorylation on DAT lateral mobility remain unexplored. Intriguingly, elevated DAT Thr53 phosphorylation is evident in DAT Val559 knock-in mice[21] in concert with elevated DAT Val559 surface expression and ADE. Thus, we explored a possible contribution of Ser53 phosphorylation to DAT membrane mobility. Upon generating diffusion profiles for DAT Ala559 and DAT Val559 expressing phosphorylation-occluded (S53A) and phosphomimetic (S53D) mutations, we observed a significant increase in D_{1-3} and 5 s displacements comparing DAT Ala559,Asp53 to DAT Ala559 populations, whereas DAT Val559,Asp53 exhibited no significant difference in D_{1-3} or 5 s displacements compared to those of DAT Val559 populations (Figure 5b, c).

Additionally, we observed that the DAT Val559,Ala53 mutant exhibited lower D_{1-3} and 5 s displacements compared

DOI: 10.1021/acschemneuro.8b00350
ACS Chem. Neurosci. 2019, 10, 460–471

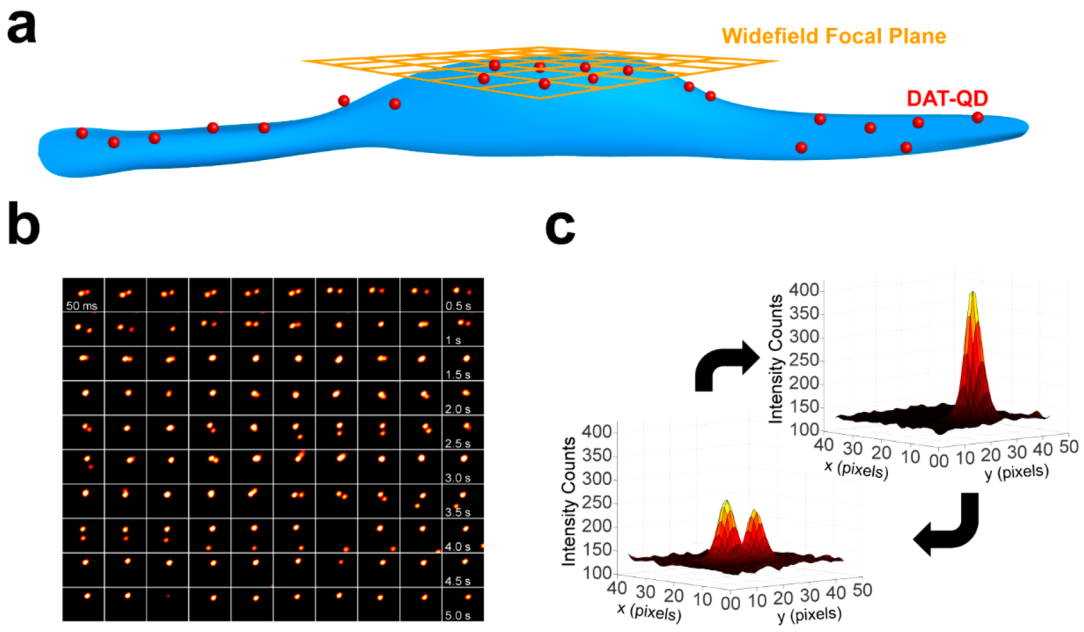

Figure 6. Intensity-based widefield imaging analysis reveals clusters at the apical cell surface. (a) Cartoon outlining the experimental widefield focal plane (orange) and DAT-QD (red) localization. (b) Representative montage of widefield epifluorescence micrographs of two DAT-QD PSFs interacting over a period of 5 s. (c) 3D surface plots of representative PSFs for single DAT-QDs and DAT-QD clusters.

to those of DAT Val559. Unexpectedly, the DAT Ala559,Ala53 mutant exhibited higher D_{1-3} and faster 5 s displacements than those of DAT Ala559, which may reflect a nonspecific impact of the Ala53 substitution on the membrane transporter diffusion. Nonetheless, occluding Ser53 phosphorylation in DAT Val559 with the Ala53 substitution resulted in diffusion coefficients comparable to those of DAT Ala559, consistent with a model where elevated phosphorylation at Ser53 in DAT Val559 is essential to the mutant's increased lateral mobility. Given that phosphorylation at distal N-terminal Ser residues as well as at Ser53 appears required for increased lateral mobility of DAT Val559, we suggest that these sites may "communicate" with each other through either transmitted conformational changes in the N-terminus or through changes in protein associations that impact transporter lateral mobility. In this regard, a number of DAT-associated proteins interact with the N-terminus including D2Rs, syntaxin 1A, and kappa opioid receptors.[49,59,60] Future studies of DAT Val559 lateral mobility should explore contributions of disrupted associations of one or more of these proteins.

DAT Val559 Exhibits Reduced Clustering at the Apical Surface of HEK-293 Cells. Several groups demonstrated that DAT undergoes oligomerization via various biochemical and optical approaches.[61−65] A more recent superresolution microscopy study demonstrated that DAT proteins are organized into functional, cholesterol-dependent nanodomains in both transfected CAD cells and dopamine neurons.[66] Moreover, transmembrane domain 12 (TM12), where the Ala559Val mutation is located, has been suggested to support dimer formation in DAT via *in silico* experiments as well as serotonin transporter (SERT) proteins via *in vitro* and *in silico* studies.[67−69] To explore the possibility of the Ala559Val mutation altering DAT clustering, we evaluated DAT Val559 clustering at the apical surface of HEK-293 cells by widefield epifluorescence microscopy. Consistent with our tracking experiments, we treated cells expressing DAT Ala559 and DAT Val559 with 100 nM IDT444 and <0.1 nM QD. Briefly, we analyzed clusters by an in house-developed intensity-based algorithm (see Materials and Methods, Figure 6a) where integrated density (ID) values were obtained by integrating point spread functions (PSF) from acquired images (Figure 6b, c). Higher ID values indicate the presence of clustered DAT-QDs (Figure 6c). For the best visualization of clusters, TALM reconstructed maps are provided (Figure 7a) for both DAT Ala559 and DAT Val559. We fit ID distributions with a lognormal function and used quantile-quantile (Q-Q) plots to compare ID values that fall outside of the fit with a 99% confidence value. DAT Ala559 ID values clearly indicate a distinct population of density values that fall outside the lognormal fit in the cluster regime, unlike DAT Val559 ID values that deviate less from the reference line (Figure 7b). These findings indicate that, in addition to an increase in lateral mobility, DAT Val559 proteins appear to cluster less on the apical surface of HEK-293 cells with other labeled transporters. These changes may preclude interactions with other DAT regulators that support normal dopamine influx/efflux bias and proper regulation of the transporter by cell signaling mechanisms. Notably, studies in the literature are mixed with respect to whether cocaine impacts multimer formation with differences possibly related to expression systems, levels of DAT expressed, and methods for multimer capture.[63,64,70−72] Although we used low concentrations of IDT444-conjugated QDs to afford labeling of a small number of targets, additional studies are needed to know whether the binding of probes to these transporters has effects on multimer formation probability on its own. Studies using TIRF approaches with GFP-tagged transporters in the presence and absence of IDT444 present one possible route to explore this possibility.[73]

In the model suggesting that alterations in cholesterol may indirectly influence DAT Val559 engagement in multi-transporter clusters, conformational changes and/or steric clashes that DAT Val559 imparts on TM12 may shift the equilibrium from a stabilized clustered state in membrane rafts

DOI: 10.1021/acschemneuro.8b00350
ACS Chem. Neurosci. 2019, 10, 460−471

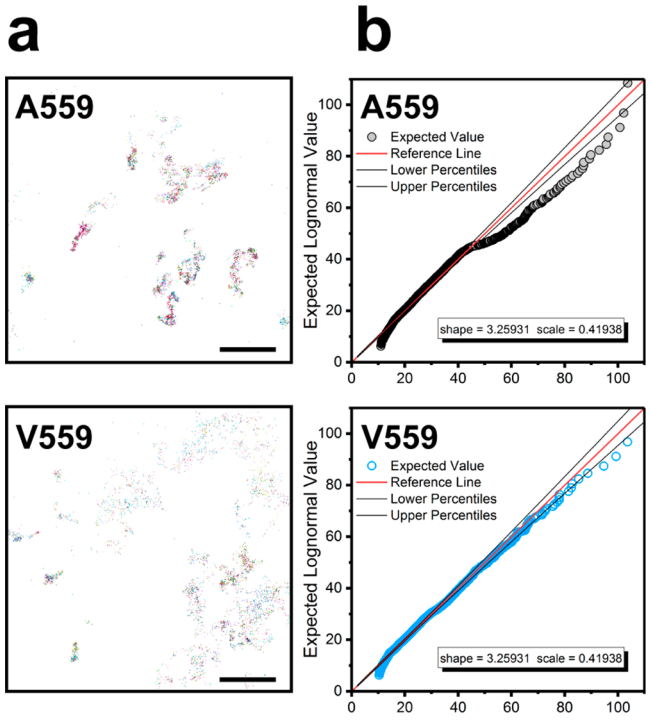

Figure 7. DAT Val559 has a lower propensity to reside in clusters at the apical surface of HEK-293 cells. (a) TALM reconstructions of DAT Ala559-QD and DAT Val559-QD PSFs from 1000-frame time series (scale bars = 2 μm). Q-Q plots (99% confidence intervals, black) of background-subtracted integrated intensity values for DAT Ala559 and DAT Val559. Upper and lower percentiles are calculated with a 99% confidence. N_{A559} = 1871, N_{V559} = 1864, 26 cells analyzed.

toward a more mobile, efflux-prone dissociated state. This would agree with the idea explored by Sitte and Freissmuth in which oligomerization acts as an important factor in reverse dopamine transport.[74] Such modification in the DAT membrane lipid environment could affect the efficacy of DAT regulation by endogenous G protein coupled receptors, such as D2R, that result in dysfunctional DAT Val559 phenotypes. Another component that could be affecting DAT clustering is phosphatidylinositol 4,5-biphosphate (PIP_2) interaction with the N-terminus of Val559. Interestingly, an unphosphorylated DAT N-terminus interacts with PIP_2*in silico*,[75] which the Galli group reported enables consequent AMPH-induced efflux.[76] The possibility of impaired efflux as a result of Val559 mistargeting PIP_2 pools cannot be easily reconciled with the observation of PIP_2 electrostatic interaction with the N-terminus being necessary for AMPH-induced efflux.[76] However, considering the phosphorylation status of DAT is important in PIP_2 binding and direct PIP_2 binding has been shown to facilitate membrane oligomerization of SERT,[73] we cannot exclude the possibility of impaired interaction between the DAT Val559 and PIP_2.

CONCLUSIONS

Neuropsychiatric disease-derived DAT missense mutations demonstrate both trafficking-dependent and -independent DAT modes of transporter dysfunction, reinforcing perturbed synaptic dopamine homeostasis as a risk determinant for neuropsychiatric disease. Although the underlying molecular mechanisms of DAT dysregulation in neuropsychiatric disorders remain to be fully elucidated, recent evidence suggests that disrupted DAT membrane microdomain compartmentalization is potentially a common culprit of DAT-mediated dopamine pathology.[26,77] Previously, we demonstrated that the ADHD-associated DAT coding Cys615 demonstrates alterations in membrane lateral mobility. Here, we provide the first single molecule tracking evidence for the DAT Val559 variant, a mutation found in subjects with ADHD, ASD, and BPD. Like DAT Cys615, DAT Val559 is more mobile compared to DAT under basal conditions. Longstanding evidence indicating that PKC mediates N-terminal phosphorylation of DAT at Ser and Thr residues,[5] and our observation of the DAT Val559 variant exhibiting altered diffusion rates, led us to perform pharmacological investigation of requirements for PKC-mediated phosphorylation. We demonstrate that DAT Val559 mobility is unresponsive to PKC activation but is attenuated by a potent and selective PKCβ inhibitor. Furthermore, DAT phosphomimicked at distal serine residues is more mobile, supporting N-terminal phosphorylation as one determinant of DAT membrane diffusion. Adding to the growing appreciation of the role of Ser/Thr53 phosphorylation in DAT function, we provide evidence that phosphorylation at this site mobilizes DAT for increased lateral diffusion, effects (phosphorylation and mobilization) instituted constitutively in the DAT Val559 variant. We report here the first experimental evidence of reduced DAT Val559 clustering related to aberrant membrane mobility.

Several groups have reported PKC modulation of DAT endocytic trafficking observed in heterologous cells to be absent in cultured midbrain neurons.[24,78−80] In contrast, Gabriel et al. recently reported PKC-mediated action on DAT trafficking observed intact striatal slices.[23] It is possible that some of this discrepancy may derive from culture versus slice approaches or the study of circuits that differentially support regulated DAT trafficking. For instance, Gowrishankar et al. found in studies of acute brain slices that D2R-dependent DAT trafficking occurs in dorsal but not ventral striatum.[21] Currently, the degree to which Val559 variant proteins diffuse and cluster *in vivo* is unknown, though this is a goal for our efforts moving forward.

As the ADHD-associated DAT Cys615 variant also demonstrates increased lateral mobility,[26] disrupted membrane localization may be a common attribute of disease-associated changes in neurotransmitter transporter availability and/or function. Beyond this more general conclusion, our results reveal previously unreported perturbations of the membrane dynamics DAT Val559 variant implicating PKCβ activation as an important determinant of transporter lateral mobility. Future studies are needed to dissect whether altered DAT Val559 membrane dynamics are a consequence of disrupted interactions between membrane domains enriched with cholesterol and/or PIP_2. Resolution of this question may lead to new opportunities for neuropsychiatric disease intervention.

MATERIALS AND METHODS

Materials. AmpQD-655, SavQD-605, and SavQD655 were purchased from Invitrogen. DMEM, fetal bovine serum (Gibco), phosphate buffer saline (PBS, w/o Ca^{2+}, Mg^{2+}), penicillin/streptomycin, and Lipofectamine 3000 were purchased from ThermoFisher. EMEM was purchased from VWR. MatTek dishes were purchased from MatTek directly. Laminin (Millipore), phorbol-12-myristate-13-acetate (PMA) (Sigma), and poly-D-lysine (Sigma) were

DOI: 10.1021/acschemneuro.8b00350
ACS Chem. Neurosci. 2019, 10, 460−471

purchased from Millipore Sigma. IDT307 (Blakely et al., 2011, U.S. Patent Number 7947255 B2) and IDT444 were synthesized in the Rosenthal Lab by Dr. Ian D. Tomlinson.[37]

Coding Variant Constructs. pcDNA3.1(+) DAT and pcDNA3.1(+) DAT Val559 constructs were previously detailed.[15] yfpsyndat (Addgene plasmid # 19991) and YFP-synDAT-S/D (Addgene plasmid # 48793) were gifts from Jonathan Javitch, Ph.D. at Columbia University. Q5 site directed mutagenesis (NEB Inc.) was used to generate hDAT A53 and D53 on both the hDAT and hDAT A559V plasmid with forward primer RB5576 5′-CCCGCGGCA-GgccCCCGTGGAGG-3′ and RB5578 5′-CCCGCGGCAGgacCCC-GTGGAGG-3′, respectively, and reverse primer RB5577 5′-TTGG-TGAGGGTGGAGCTGG-3′.

Cell Culture. HEK-293 cells were a kind gift from Eva Harth, Ph.D. at Vanderbilt University, and SK-N-MC cells were kindly provided by Jerry Chang, Ph.D. at the Rockefeller University Laboratory of Molecular and Cellular Neuroscience. HEK-293 and SK-N-MC cells were maintained in DMEM and EMEM, respectively, with 2 mM/L glutamine, 10% fetal bovine serum (FBS), and 1% penicillin/streptomycin. Both cell cultures were transiently transfected 24 h prior to labeling at 1 μg DNA:3 μL Lipofectamine 3000 ratio.

QD Labeling. DAT-expressing HEK-293 and SK-N-MC cells were plated on MatTek No. 1.5 coverslips coated with poly-D-lysine and laminin, respectively. QD labeling was employed following a two-step protocol previously outlined.[81] Briefly, cells in 2 mL of full growth medium were spiked with 20 μL of 10 μM IDT444 suspended in PBS (w/o Ca^{2+}, Mg^{2+}) and incubated at 37 °C and 5% CO_2 for 10 min. Three washes with warm DMEM Fluorobrite were performed prior to treating cells with 10 pM SavQD 2% dialyzed FBS in DMEM Fluorobrite. The QD-IDT444 DAT-labeled cells were washed three times with warm DMEM Fluorobrite. Activation of PKC and inhibition of PKCβ were performed by administering 100 nM PMA 30 min prior to washing and 1 μM Enz prior to PMA treatment, respectively. PMA- and Enz-treated cells were washed an additional 3 times with warm DMEM Fluorobrite. At the microscope, IDT307 was added to the MatTek dish prior to imaging.

Microscopy. Time-series images were generated by TIRF and widefield epifluorescence microscopy on a Nikon Eclipse Ti-E inverted microscope equipped with an Andor Zyla 4.2 PLUS sCMOS camera and viewed with an Apo TIRF 60×/1.49 NA oil objective. Excitation at 488 nm was sourced by a Nikon LU-NV laser unit. YFP-DAT and IDT307 emissions were collected with a 525 ± 18 nm emission filter. SavQD-605 and SavQD-655 signals were collected with 603 ± 15 nm and 655 ± 15 nm emission filters, respectively. For SPT experiments, time series were produced at a 10 Hz frame rate. For clustering experiments, time series were produced at a 17 Hz frame rate.

Single Particle Tracking Analysis. Raw TIFF stacks were extracted from Nikon Elements ndl files in Fiji, an ImageJ distribution (National Institutes of Health, Bethesda, MD). Trajectories were compiled from these raw data given the conditions that (i) the particle emission is intermittent to ensure discrimination of single particles, (ii) the blinking gap is less than 10 frames, (iii) the PSF is located within a 3 × 3 pixel area surrounding the PSF location from the previous frame, and (iv) the trajectory persists at least 50 frames. Mean square displacement, $\langle r^2(n\delta t)\rangle$, values were calculated for each of the trajectories collected for time intervals of 0.1−1.5 s in 0.1 s intervals via

$$\langle r^2(n\delta t)\rangle = \frac{1}{N-n}\sum_{j=0}^{N-n-1}\{[x(j\delta t + n\delta t) - x(j\delta t)]^2 + [y(j\delta t + n\delta t) - y(j\delta t)]^2\} \quad (n = 0,1,2, ..., N-1)$$

where δt is the temporal resolution, $(x(j\delta t), x(j\delta t))$ is the coordinate at $t = j\delta t$, and N is the number of total frames recorded during a single trajectory.

Diffusion coefficients (D_{1-3}) were determined from the linear fits of the first three MSD values in the algorithm

$$r^2(t)_{1-3} = 4D_{1-3}t + 4\sigma^2$$

where σ is the uncertainty of particle localization. The uncertainty, dependent on the signal-to-noise ratio (SNR) and limited by the diffraction limit using visible light, was estimated by $\Delta\sigma \approx \omega/SNR$, where ω is approximately the widefield mode diffraction limit and SNR values for QD emitters exited by an evanescent field in TIRF mode range between 20 and 30. D_{1-3} values were populated, and a significant difference between distributions was determined by one-way ANOVA followed by Bonferroni's multiple comparison test. 5 s displacement vectors were obtained by indexing particle coordinates after 50 frames and normalizing to the particle origin. Populated 5 s displacement values were analyzed by unpaired Student's t test. All analysis was performed and automated by MATLAB codes. For extensive detail regarding microscopy and analysis in SPT experiments, see Chang and Rosenthal et al.[82]

Cluster Analysis. Raw TIFF stacks were extracted from Nikon Elements ndl files in Fiji. PSF centroids were subsequently identified and indexed. For the intensity of each PSF to be quantified, ID values were calculated by integrating raw intensity values in a 5 × 5 pixel matrix and normalized to the particle centroid coordinate. Because background in widefield mode is heterogeneous due to emission from QDs outside of the focal plane, background values were calculated by averaging intensity counts of a 9 × 9 pixel parameter centered around each centroid. Raw IDs were then corrected by their assigned backgrounds. All analysis was performed and automated by an in-house MATLAB script. The QuickPALM plugin in Fiji was used to generate TALM images.

■ ASSOCIATED CONTENT

Supporting Information

The Supporting Information is available free of charge on the ACS Publications website at DOI: 10.1021/acschemneuro.8b00350.

Table of N values (Trajectories, Table S1), SPT data of (i) DAT vs DAT Val559 in basal conditions (Figure S1), (ii) under PMA and enzastaurin treatments (Figure S2), and (iii) YFP-DAT vs YFP-DAT S/D in SK-N-MC cells (PDF)

Example time-lapse image series of DAT-QD complexes in live SK-N-MC cells (AVI)

■ AUTHOR INFORMATION

Corresponding Author

*E-mail: sandra.j.rosenthal@vanderbilt.edu.

ORCID

Lucas B. Thal: 0000-0002-4369-7827

Randy D. Blakely: 0000-0002-2182-6966

Sandra J. Rosenthal: 0000-0002-4576-5854

Author Contributions

L.B.T., R.D.B., and S.J.R. conceived and planned experiments. I.D.T. synthesized IDT444 used in all experiments. L.B.T. cultured transfected cells and carried out single particle tracking experiments with the exception of YFP-DAT vs YFP-DAT S/D experiments which O.K. performed. L.B.T. also carried out clustering experiments, performed statistical analysis, and generated figures. M.A.Q. generated the DAT S53,A559, DAT D53,A559, DAT S53,V559, DAT D53,V559 plasmids. L.B.T., I.D.T., M.A.Q., O.K., R.D.B., and S.J.R. contributed to interpreting the results. L.B.T. took lead in writing the manuscript. All authors contributed to editing the manuscript.

Notes

The authors declare no competing financial interest.

DOI: 10.1021/acschemneuro.8b00350
ACS Chem. Neurosci. 2019, 10, 460−471

■ ACKNOWLEDGMENTS

Imaging was performed in the VUMC Cell Imaging Resource Center (supported by NIH grants CA68485, DK20593, DK20953, DK58404, DK59637, and EY08126). LBT was supported by the NIH Chemistry-Biology Interface training grant (NIH T32GM065086-14). RDB was supported by NIH grant MH105094.

■ REFERENCES

(1) Giros, B., and Caron, M. G. (1993) Molecular characterization of the dopamine transporter. *Trends Pharmacol. Sci. 14* (2), 43−49.
(2) Palmiter, R. D. (2008) Dopamine signaling in the dorsal striatum Is essential for motivated behaviors. *Ann. N. Y. Acad. Sci. 1129* (1), 35−46.
(3) Bannon, M. J., Michelhaugh, S. K., Wang, J., and Sacchetti, P. (2001) The human dopamine transporter gene: gene organization, transcriptional regulation, and potential involvement in neuropsychiatric disorders. *Eur. Neuropsychopharmacol. 11* (6), 449−455.
(4) Howes, O., McCutcheon, R., and Stone, J. (2015) Glutamate and dopamine in schizophrenia: An update for the 21st century. *J. Psychopharmacol. 29* (2), 97−115.
(5) Bermingham, D. P., and Blakely, R. D. (2016) Kinase-dependent regulation of monoamine neurotransmitter transporters. *Pharmacol. Rev. 68* (4), 888−953.
(6) Nutt, D. J., Lingford-Hughes, A., Erritzoe, D., and Stokes, P. R. A. (2015) The dopamine theory of addiction: 40 years of highs and lows. *Nat. Rev. Neurosci. 16*, 305.
(7) Giros, B., Jaber, M., Jones, S. R., Wightman, R. M., and Caron, M. G. (1996) Hyperlocomotion and indifference to cocaine and amphetamine in mice lacking the dopamine transporter. *Nature 379*, 606.
(8) Gainetdinov, R. R., Jones, S. R., and Caron, M. G. (1999) Functional hyperdopaminergia in dopamine transporter knock-out mice. *Biol. Psychiatry 46* (3), 303−311.
(9) Ralph, R. J., Paulus, M. P., Fumagalli, F., Caron, M. G., and Geyer, M. A. (2001) Prepulse inhibition deficits and perseverative motor patterns in dopamine transporter knock-out mice: Differential effects of D1 and D2 receptor antagonists. *J. Neurosci. 21* (1), 305−313.
(10) Mazei-Robison, M. S., Couch, R. S., Shelton, R. C., Stein, M. A., and Blakely, R. D. (2005) Sequence variation in the human dopamine transporter gene in children with attention deficit hyperactivity disorder. *Neuropharmacology 49* (6), 724−736.
(11) Grünhage, F., Schulze, T. G., Müller, D. J., Lanczik, M., Franzek, E., Albus, M., Borrmann-Hassenbach, M., Knapp, M., Cichon, S., Maier, W., Rietschel, M., Propping, P., and Nöthen, M. M. (2000) Systematic screening for DNA sequence variation in the coding region of the human dopamine transporter gene (DAT1). *Mol. Psychiatry 5*, 275.
(12) Hahn, M. K., and Blakely, R. D. (2007) The functional impact of SLC6 transporter genetic variation. *Annu. Rev. Pharmacol. Toxicol. 47* (1), 401−441.
(13) Hansen, F. H., Skjørringe, T., Yasmeen, S., Arends, N. V., Sahai, M. A., Erreger, K., Andreassen, T. F., Holy, M., Hamilton, P. J., Neergheen, V., Karlsborg, M., Newman, A. H., Pope, S., Heales, S. J. R., Friberg, L., Law, I., Pinborg, L. H., Sitte, H. H., Loland, C., Shi, L., Weinstein, H., Galli, A., Hjermind, L. E., Møller, L. B., and Gether, U. (2014) Missense dopamine transporter mutations associate with adult parkinsonism and ADHD. *J. Clin. Invest. 124* (7), 3107−3120.
(14) Kurian, M. A., Gissen, P., Smith, M., Heales, S. J. R., and Clayton, P. T. (2011) The monoamine neurotransmitter disorders: an expanding range of neurological syndromes. *Lancet Neurol. 10* (8), 721−733.
(15) Hamilton, P. J., Campbell, N. G., Sharma, S., Erreger, K., Herborg Hansen, F., Saunders, C., Belovich, A. N., Consortium, N. A. A. S., Sahai, M. A., Cook, E. H., Gether, U., McHaourab, H. S., Matthies, H. J. G., Sutcliffe, J. S., and Galli, A. (2013) *De novo* mutation in the dopamine transporter gene associates dopamine dysfunction with autism spectrum disorder. *Mol. Psychiatry 18*, 1315.
(16) Wu, S., Fagan, R. R., Uttamapinant, C., Lifshitz, L. M., Fogarty, K. E., Ting, A. Y., and Melikian, H. E. (2017) The dopamine transporter recycles via a retromer-dependent postendocytic mechanism: Tracking studies using a novel fluorophore-coupling approach. *J. Neurosci. 37* (39), 9438−9452.
(17) Wu, S., Bellve, K. D., Fogarty, K. E., and Melikian, H. E. (2015) Ack1 is a dopamine transporter endocytic brake that rescues a trafficking-dysregulated ADHD coding variant. *Proc. Natl. Acad. Sci. U. S. A. 112* (50), 15480−15485.
(18) Wheeler, D. S., Underhill, S. M., Stolz, D. B., Murdoch, G. H., Thiels, E., Romero, G., and Amara, S. G. (2015) Amphetamine activates Rho GTPase signaling to mediate dopamine transporter internalization and acute behavioral effects of amphetamine. *Proc. Natl. Acad. Sci. U. S. A. 112* (51), E7138−E7147.
(19) Zhu, S., Zhao, C., Wu, Y., Yang, Q., Shao, A., Wang, T., Wu, J., Yin, Y., Li, Y., Hou, J., Zhang, X., Zhou, G., Gu, X., Wang, X., Bustelo, X. R., and Zhou, J. (2015) Identification of a Vav2-dependent mechanism for GDNF/Ret control of mesolimbic DAT trafficking. *Nat. Neurosci. 18*, 1084.
(20) Block, E. R., Nuttle, J., Balcita-Pedicino, J. J., Caltagarone, J., Watkins, S. C., Sesack, S. R., and Sorkin, A. (2015) Brain region-specific trafficking of the dopamine transporter. *J. Neurosci. 35* (37), 12845−12858.
(21) Gowrishankar, R., Gresch, P. J., Davis, G. L., Katamish, R. M., Riele, J. R., Stewart, A. M., Vaughan, R. A., Hahn, M. K., and Blakely, R. D. (2018) Region-specific regulation of presynaptic dopamine homeostasis by D2 autoreceptors shapes the *In Vivo* impact of the neuropsychiatric disease-associated DAT variant Val559. *J. Neurosci.*, 0055-18.
(22) Furman, C. A., Chen, R., Guptaroy, B., Zhang, M., Holz, R. W., and Gnegy, M. (2009) Dopamine and amphetamine rapidly increase dopamine transporter trafficking to the surface: Live-cell imaging using total internal reflection fluorescence microscopy. *J. Neurosci. 29* (10), 3328−3336.
(23) Gabriel, L. R., Wu, S., Kearney, P., Bellvé, K. D., Standley, C., Fogarty, K. E., and Melikian, H. E. (2013) Dopamine transporter endocytic trafficking in striatal dopaminergic neurons: differential dependence on dynamin and the actin cytoskeleton. *J. Neurosci. 33* (45), 17836−17846.
(24) Eriksen, J., Rasmussen, S. G. F., Rasmussen, T. N., Vaegter, C. B., Cha, J. H., Zou, M.-F., Newman, A. H., and Gether, U. (2009) Visualization of dopamine transporter trafficking in live neurons by use of fluorescent cocaine analogs. *J. Neurosci. 29* (21), 6794−6808.
(25) Sorkina, T., Caltagarone, J., and Sorkin, A. (2013) Flotillins regulate membrane mobility of the dopamine transporter but are not required for its protein kinase C dependent endocytosis. *Traffic 14* (6), 709−724.
(26) Kovtun, O., Sakrikar, D., Tomlinson, I. D., Chang, J. C., Arzeta-Ferrer, X., Blakely, R. D., and Rosenthal, S. J. (2015) Single-quantum-dot tracking reveals altered membrane dynamics of an attention-deficit/hyperactivity-disorder-derived dopamine transporter coding variant. *ACS Chem. Neurosci. 6* (4), 526−534.
(27) Rosenthal, S. J., Chang, J. C., Kovtun, O., McBride, J. R., and Tomlinson, I. D. (2011) Biocompatible quantum dots for biological applications. *Chem. Biol. 18* (1), 10−24.
(28) Dahan, M., Levi, S., Luccardini, C., Rostaing, P., Riveau, B., and Triller, A. (2003) Diffusion dynamics of glycine receptors revealed by single-quantum dot tracking. *Science 302* (5644), 442−445.
(29) Bouzigues, C., Morel, M., Triller, A., and Dahan, M. (2007) Asymmetric redistribution of GABA receptors during GABA gradient sensing by nerve growth cones analyzed by single quantum dot imaging. *Proc. Natl. Acad. Sci. U. S. A. 104* (27), 11251−11256.
(30) Frischknecht, R., Heine, M., Perrais, D., Seidenbecher, C. I., Choquet, D., and Gundelfinger, E. D. (2009) Brain extracellular matrix affects AMPA receptor lateral mobility and short-term synaptic plasticity. *Nat. Neurosci. 12* (7), 897−904.

DOI: 10.1021/acschemneuro.8b00350
ACS Chem. Neurosci. 2019, 10, 460−471

(31) Chang, J. C., Tomlinson, I. D., Warnement, M. R., Ustione, A., Carneiro, A. M. D., Piston, D. W., Blakely, R. D., and Rosenthal, S. J. (2012) Single molecule analysis of serotonin transporter regulation using antagonist-conjugated quantum dots reveals restricted, p38 MAPK-dependent mobilization underlying uptake activation. *J. Neurosci. 32* (26), 8919−8929.
(32) Bailey, D. M., Catron, M. A., Kovtun, O., Macdonald, R. L., Zhang, Q., and Rosenthal, S. J. (2018) Single quantum dot tracking reveals serotonin transporter diffusion dynamics are correlated with cholesterol-sensitive threonine 276 phosphorylation status in primary midbrain neurons. *ACS Chem. Neurosci.*, in press DOI: 10.1021/acschemneuro.8b00214.
(33) McBride, J., Treadway, J., Feldman, L. C., Pennycook, S. J., and Rosenthal, S. J. (2006) Structural basis for near unity quantum yield core/shell nanostructures. *Nano Lett. 6* (7), 1496−1501.
(34) Kovtun, O., Tomlinson, I. D., Bailey, D. M., Thal, L. B., Ross, E. J., Harris, L., Frankland, M. P., Ferguson, R. S., Glaser, Z., Greer, J., and Rosenthal, S. J. (2018) Single quantum dot tracking illuminates neuroscience at the nanoscale. *Chem. Phys. Lett. 706*, 741−752.
(35) Choquet, D., and Triller, A. (2003) The role of receptor diffusion in the organization of the postsynaptic membrane. *Nat. Rev. Neurosci. 4*, 251.
(36) Triller, A., and Choquet, D. (2008) New concepts in synaptic biology derived from single-molecule imaging. *Neuron 59* (3), 359−374.
(37) Kahlig, K. M., Lute, B. J., Wei, Y., Loland, C. J., Gether, U., Javitch, J. A., and Galli, A. (2006) Regulation of dopamine transporter trafficking by intracellular amphetamine. *Mol. Pharmacol. 70* (2), 542−548.
(38) Gussin, H. A., Tomlinson, I. D., Cao, D., Qian, H., Rosenthal, S. J., and Pepperberg, D. R. (2013) Quantum dot conjugates of GABA and muscimol: Binding to $\alpha1\beta2\gamma2$ and $\rho1$ $GABA_A$ receptors. *ACS Chem. Neurosci. 4* (3), 435−443.
(39) Gussin, H. A., Tomlinson, I. D., Little, D. M., Warnement, M. R., Qian, H., Rosenthal, S. J., and Pepperberg, D. R. (2006) Binding of muscimol-conjugated quantum dots to $GABA_C$ receptors. *J. Am. Chem. Soc. 128* (49), 15701−15713.
(40) Kovtun, O., Tomlinson, I. D., Sakrikar, D. S., Chang, J. C., Blakely, R. D., and Rosenthal, S. J. (2011) Visualization of the cocaine-sensitive dopamine transporter with ligand-conjugated quantum dots. *ACS Chem. Neurosci. 2* (7), 370−378.
(41) Rosenthal, S. J., Tomlinson, I., Adkins, E. M., Schroeter, S., Adams, S., Swafford, L., McBride, J., Wang, Y., DeFelice, L. J., and Blakely, R. D. (2002) Targeting cell surface receptors with ligand-conjugated nanocrystals. *J. Am. Chem. Soc. 124* (17), 4586−4594.
(42) Bowton, E., Saunders, C., Reddy, I. A., Campbell, N. G., Hamilton, P. J., Henry, L. K., Coon, H., Sakrikar, D., Veenstra-VanderWeele, J. M., Blakely, R. D., Sutcliffe, J., Matthies, H. J. G., Erreger, K., and Galli, A. (2014) SLC6A3 coding variant Ala559Val found in two autism probands alters dopamine transporter function and trafficking. *Transl. Psychiatry 4*, No. e464.
(43) Mergy, M. A., Gowrishankar, R., Gresch, P. J., Gantz, S. C., Williams, J., Davis, G. L., Wheeler, C. A., Stanwood, G. D., Hahn, M. K., and Blakely, R. D. (2014) The rare DAT coding variant Val559 perturbs DA neuron function, changes behavior, and alters *in vivo* responses to psychostimulants. *Proc. Natl. Acad. Sci. U. S. A. 111* (44), E4779−E4788.
(44) Davis, G. L., Stewart, A., Stanwood, G. D., Gowrishankar, R., Hahn, M. K., and Blakely, R. D. (2018) Functional coding variation in the presynaptic dopamine transporter associated with neuropsychiatric disorders drives enhanced motivation and context-dependent impulsivity in mice. *Behav. Brain Res. 337*, 61−69.
(45) Mazei-Robison, M. S., Bowton, E., Holy, M., Schmudermaier, M., Freissmuth, M., Sitte, H. H., Galli, A., and Blakely, R. D. (2008) Anomalous dopamine release associated with a human dopamine transporter coding variant. *J. Neurosci. 28* (28), 7040−7046.
(46) Mazei-Robison, M. S., and Blakely, R. D. (2005) Expression studies of naturally occurring human dopamine transporter variants identifies a novel state of transporter inactivation associated with Val382Ala. *Neuropharmacology 49* (6), 737−749.
(47) Herborg, F., Andreassen, T. F., Berlin, F., Loland, C. J., and Gether, U. (2018) Neuropsychiatric disease-associated genetic variants of the dopamine transporter display heterogeneous molecular phenotypes. *J. Biol. Chem. 293*, 7250.
(48) Bolan, E. A., Kivell, B., Jaligam, V., Oz, M., Jayanthi, L. D., Han, Y., Sen, N., Urizar, E., Gomes, I., Devi, L. A., Ramamoorthy, S., Javitch, J. A., Zapata, A., and Shippenberg, T. S. (2007) D_2 receptors regulate dopamine transporter function via an extracellular signal-regulated kinases 1 and 2-dependent and phosphoinositide 3 kinase-independent mechanism. *Mol. Pharmacol. 71* (5), 1222−1232.
(49) Lee, F. J., Pei, L., Moszczynska, A., Vukusic, B., Fletcher, P. J., and Liu, F. (2007) Dopamine transporter cell surface localization facilitated by a direct interaction with the dopamine D2 receptor. *EMBO J. 26* (8), 2127−2136.
(50) Bowton, E., Saunders, C., Erreger, K., Sakrikar, D., Matthies, H. J., Sen, N., Jessen, T., Colbran, R. J., Caron, M. G., Javitch, J. A., Blakely, R. D., and Galli, A. (2010) Dysregulation of dopamine transporters via dopamine D2 autoreceptors triggers anomalous dopamine efflux associated with attention-deficit hyperactivity disorder. *J. Neurosci. 30* (17), 6048−6057.
(51) Blakely, R. D., Mason, J. N., Tomlinson, I. D., and Rosenthal, S. J. Fluorescent substrates for neurotransmitter transporters. Google Patents US8647827B2, 2011.
(52) Mason, J. N., Farmer, H., Tomlinson, I. D., Schwartz, J. W., Savchenko, V., DeFelice, L. J., Rosenthal, S. J., and Blakely, R. D. (2005) Novel fluorescence-based approaches for the study of biogenic amine transporter localization, activity, and regulation. *J. Neurosci. Methods 143* (1), 3−25.
(53) Johnson, L. A. A., Guptaroy, B., Lund, D., Shamban, S., and Gnegy, M. E. (2005) Regulation of amphetamine-stimulated dopamine efflux by protein kinase C β. *J. Biol. Chem. 280* (12), 10914−10919.
(54) Chen, R., Furman, C. A., Zhang, M., Kim, M. N., Gereau, R. W., Leitges, M., and Gnegy, M. E. (2009) Protein kinase C β is a critical regulator of dopamine transporter trafficking and regulates the behavioral response to amphetamine in mice. *J. Pharmacol. Exp. Ther. 328* (3), 912−920.
(55) Zestos, A. G., Mikelman, S. R., Kennedy, R. T., and Gnegy, M. E. (2016) PKCβ inhibitors attenuate amphetamine-stimulated dopamine efflux. *ACS Chem. Neurosci. 7* (6), 757−766.
(56) Daniels, G. M., and Amara, S. G. (1999) Regulated trafficking of the human dopamine transporter: Clatherin-mediated internalization and lysosomal degradation in response to phorbol esters. *J. Biol. Chem. 274* (50), 35794−35801.
(57) Carvelli, L., Morón, J. A., Kahlig, K. M., Ferrer, J. V., Sen, N., Lechleiter, J. D., Leeb-Lundberg, L. M., Merrill, G., Lafer, E. M., Ballou, L. M., Shippenberg, T. S., Javitch, J. A., Lin, R. Z., and Galli, A. (2002) PI 3-kinase regulation of dopamine uptake. *J. Neurochem. 81* (4), 859−869.
(58) Foster, J. D., Yang, J.-W., Moritz, A. E., ChallaSivaKanaka, S., Smith, M. A., Holy, M., Wilebski, K., Sitte, H. H., and Vaughan, R. A. (2012) Dopamine transporter phosphorylation site threonine 53 regulates substrate reuptake and amphetamine-stimulated efflux. *J. Biol. Chem. 287* (35), 29702−29712.
(59) Binda, F., Dipace, C., Bowton, E., Robertson, S. D., Lute, B. J., Fog, J. U., Zhang, M., Sen, N., Colbran, R. J., Gnegy, M. E., Gether, U., Javitch, J. A., Erreger, K., and Galli, A. (2008) Syntaxin 1A interaction with the dopamine transporter promotes amphetamine-induced dopamine efflux. *Mol. Pharmacol. 74* (4), 1101−1108.
(60) Kivell, B., Uzelac, Z., Sundaramurthy, S., Rajamanickam, J., Ewald, A., Chefer, V., Jaligam, V., Bolan, E., Simonson, B., Annamalai, B., Mannangatti, P., Prisinzano, T. E., Gomes, I., Devi, L. A., Jayanthi, L. D., Sitte, H. H., Ramamoorthy, S., and Shippenberg, T. S. (2014) Salvinorin A regulates dopamine transporter function via a kappa opioid receptor and ERK1/2-dependent mechanism. *Neuropharmacology 86*, 228−240.

DOI: 10.1021/acschemneuro.8b00350
ACS Chem. Neurosci. 2019, 10, 460−471

(61) Torres, G. E., Carneiro, A., Seamans, K., Fiorentini, C., Sweeney, A., Yao, W.-D., and Caron, M. G. (2003) Oligomerization and trafficking of the human dopamine transporter: Mutational analysis identifies critical domains important for the functional expression of the transporter. *J. Biol. Chem. 278* (4), 2731−2739.
(62) Sorkina, T., Doolen, S., Galperin, E., Zahniser, N. R., and Sorkin, A. (2003) Oligomerization of dopamine transporters visualized in living cells by fluorescence resonance energy transfer microscopy. *J. Biol. Chem. 278* (30), 28274−28283.
(63) Hastrup, H., Sen, N., and Javitch, J. A. (2003) The human dopamine transporter forms a tetramer in the plasma membrane: Cross-linking of a cysteine in the fourth segment is sensitive to cocaine analogs. *J. Biol. Chem. 278* (46), 45045−45048.
(64) Chen, N., and Reith, M. E. A. (2008) Substrates dissociate dopamine transporter oligomers. *J. Neurochem. 105* (3), 910−920.
(65) Egaña, L. A., Cuevas, R. A., Baust, T. B., Parra, L. A., Leak, R. K., Hochendoner, S., Peña, K., Quiroz, M., Hong, W. C., Dorostkar, M. M., Janz, R., Sitte, H. H., and Torres, G. E. (2009) Physical and functional interaction between the dopamine transporter and the synaptic vesicle protein synaptogyrin-3. *J. Neurosci. 29* (14), 4592−4604.
(66) Rahbek-Clemmensen, T., Lycas, M. D., Erlendsson, S., Eriksen, J., Apuschkin, M., Vilhardt, F., Jørgensen, T. N., Hansen, F. H., and Gether, U. (2017) Super-resolution microscopy reveals functional organization of dopamine transporters into cholesterol and neuronal activity-dependent nanodomains. *Nat. Commun. 8* (1), 740.
(67) Periole, X., Zeppelin, T., and Schiøtt, B. (2018) Dimer interface of the human serotonin transporter and effect of the membrane composition. *Sci. Rep. 8* (1), 5080.
(68) Just, H., Sitte, H. H., Schmid, J. A., Freissmuth, M., and Kudlacek, O. (2004) Identification of an additional interaction domain in transmembrane domains 11 and 12 that supports oligomer formation in the human serotonin transporter. *J. Biol. Chem. 279* (8), 6650−6657.
(69) Jayaraman, K., Morley, A. N., Szöllősi, D., Wassenaar, T. A., Sitte, H. H., and Stockner, T. (2018) Dopamine transporter oligomerization involves the scaffold domain, but spares the bundle domain. *PLoS Comput. Biol. 14* (6), No. e1006229.
(70) Anderluh, A., Klotzsch, E., Reismann, A. W. A. F., Brameshuber, M., Kudlacek, O., Newman, A. H., Sitte, H. H., and Schütz, G. J. (2014) Single molecule analysis reveals coexistence of stable serotonin transporter monomers and oligomers in the live cell plasma membrane. *J. Biol. Chem. 289*, 4387.
(71) Siciliano, C. A., Saha, K., Calipari, E. S., Fordahl, S. C., Chen, R., Khoshbouei, H., and Jones, S. R. (2018) Amphetamine reverses escalated cocaine intake via restoration of dopamine transporter conformation. *J. Neurosci. 38* (2), 484−497.
(72) Sorkina, T., Ma, S., Larsen, M. B., Watkins, S. C., and Sorkin, A. (2018) Small molecule induced oligomerization, clustering and clathrin-independent endocytosis of the dopamine transporter. *eLife 7*, No. e32293.
(73) Anderluh, A., Hofmaier, T., Klotzsch, E., Kudlacek, O., Stockner, T., Sitte, H. H., and Schütz, G. J. (2017) Direct PIP2 binding mediates stable oligomer formation of the serotonin transporter. *Nat. Commun. 8*, 14089.
(74) Sitte, H. H., and Freissmuth, M. (2015) Amphetamines, new psychoactive drugs and the monoamine transporter cycle. *Trends Pharmacol. Sci. 36* (1), 41−50.
(75) Khelashvili, G., Stanley, N., Sahai, M. A., Medina, J., LeVine, M. V., Shi, L., De Fabritiis, G., and Weinstein, H. (2015) Spontaneous inward opening of the dopamine transporter is triggered by PIP2-regulated dynamics of the N-terminus. *ACS Chem. Neurosci. 6* (11), 1825−1837.
(76) Hamilton, P. J., Belovich, A. N., Khelashvili, G., Saunders, C., Erreger, K., Javitch, J. A., Sitte, H. H., Weinstein, H., Matthies, H. J., and Galli, A. (2014) PIP_2 regulates psychostimulant behaviors through its interaction with a membrane protein. *Nat. Chem. Biol. 10* (7), 582.
(77) Robinson, S. B., Hardaway, J. A., Hardie, S. L., Wright, J., Glynn, R. M., Bermingham, D. P., Han, Q., Sturgeon, S. M., Freeman, P., and Blakely, R. D. (2017) Sequence determinants of the Caenhorhabditis elegans dopamine transporter dictating *in vivo* axonal export and synaptic localization. *Mol. Cell. Neurosci. 78*, 41−51.
(78) Sorkina, T., Miranda, M., Dionne, K. R., Hoover, B. R., Zahniser, N. R., and Sorkin, A. (2006) RNA interference screen reveals an essential role of nedd4−2 in dopamine transporter ubiquitination and endocytosis. *J. Neurosci. 26* (31), 8195−8205.
(79) Rao, A., Simmons, D., and Sorkin, A. (2011) Differential subcellular distribution of endosomal compartments and the dopamine transporter in dopaminergic neurons. *Mol. Cell. Neurosci. 46* (1), 148−158.
(80) Rao, A., Richards, T. L., Simmons, D., Zahniser, N. R., and Sorkin, A. (2012) Epitope-tagged dopamine transporter knock-in mice reveal rapid endocytic trafficking and filopodia targeting of the transporter in dopaminergic axons. *FASEB J. 26* (5), 1921−1933.
(81) Thal, L. B., Bailey, D. M., Kovtun, O., and Rosenthal, S. J. Quantum dot toolbox in membrane neurotransmitter transporter research. *Chemical and Synthetic Approaches in Membrane Biology*; Springer Protocols Handbooks, Humana Press NY: Totowa, NJ, 2017; pp 1−12.
(82) Chang, J. C., and Rosenthal, S. J. Real-time quantum dot tracking of single proteins. In *Biomedical Nanotechnology: Methods and Protocols*; Hurst, S. J., Ed.; Humana Press: Totowa, NJ, 2011; pp 51−62.

DOI: 10.1021/acschemneuro.8b00350
ACS Chem. Neurosci. 2019, 10, 460−471